

Use of oil palm frond waste to reinforce poly(lactic acid) based composites with the improvement of interfacial adhesion by alkali treatment

Nattakarn HONGSRIPHAN^{1,*}, Jidapa SUBSANGA¹, Pimpisa SUEBSAI¹, Sunisa SITTHIPONG¹, and Pajaera PATANATHABUTR¹

¹ Department of Materials Science and Engineering, Faculty of Engineering and Industrial Technology, Silpakorn University, Nakhon Pathom, 73000, Thailand

*Corresponding author e-mail: Hongsriphan_N@su.ac.th

Received date:

16 October 2021

Revised date:

16 January 2022

Accepted date:

24 January 2022

Keywords:

Wood fiber composite;
Oil palm frond;
Poly(lactic acid);
Alkali treatment

Abstract

Oil palm frond waste was used as reinforcing fibers for biodegradable poly(lactic acid) or PLA in order to produce green composites that increased the value of agricultural waste. The alkali-treated oil palm frond (OPF) fibers of 30 wt% or 40 wt% were compounded with PLA and moulded into specimens. The alkali treatment was 0 wt%, 1 wt%, 3 wt%, and 5 wt% of the fibers for compatibility improvement with PLA matrix. It was found that the alkali-treated PLA/OPF composites adding 30 wt% and 40 wt% had the flexural modulus to be about 55% and 75% higher than those without the treatment, respectively. Tensile modulus of the composites was also increased. Nevertheless, the higher rigidity composites became more brittle as evident by the fracture toughness testing. The increase of total breaking energy confirmed the better interfacial adhesion between phases as shown in SEM micrographs. The glass transition temperature (T_g) of PLA matrix in the composites was shifted to lower temperature attributed to the thermal degradation of PLA during the melt compounding confirmed by the lower degradation temperature. Increasing the alkali concentration for surface treatment caused the T_g of PLA composites to be higher, supporting that the improvement of interfacial adhesion was achieved.

1. Introduction

For the last decades, poly(lactic acid) (PLA) is one of the biodegradable polymers [1] that has been researched to investigate properties when applied into various applications. PLA is an aliphatic polyester that has properties similarly to polystyrene, such as transparent and good rigidity with brittleness. Since its chemical nature consists of the polyester linkage, the reinforcement of PLA with lignocellulosic fibers enhances mechanical properties as well as thermomechanical properties. There have been research works that attempted to produce green composites by reinforcing PLA with lignocellulosic fibers such as sisal and flax [2], eucalyptus [3], and pulp [4].

The reinforcement of lignocellulosic fibers into PLA matrix could provide the biodegradable composites that would possibly replace the use of natural softwood. For example, PLA/lignocellulosic fiber composite is an interesting alternative material to replace traditional wood panels for interior decoration. It offers several advantages, such as lighter, resistant to rot or decay, and can be shaped using conventional woodworking tool. Sripathi Dev Sharma Koppa and Anil N. Netravali [5] reviewed and provided a brief summary of the mechanical responses of different types of natural fiber reinforced green composites using biodegradable resins and their commercial practicability in primary and secondary structural applications. They emphasized on the environmentally beneficial characteristics such as

biodegradability that could reduce the landfill loads and lead to significant reduction in carbon foot-print.

Oil palm tree is one of the economic tropical trees that gardeners in the Southeast Asia harvests oil palm for producing various products such as frying oil, food products, cosmetics, and biodiesel. Typically, oil palm fronds [6] have to be cut out throughout the tree's life cycle for keeping good health. Thus, these oil palm fronds become agricultural waste. Gardeners reuse them as organic fertilizer sources in the garden that reduce use of chemical fertilizer which could contaminate

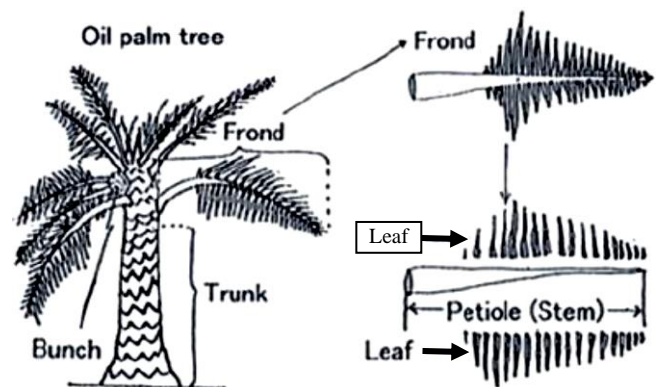


Figure 1. Oil palm tree showing oil palm frond consists of leaf and stem. Oil palm frond fibers (OPF) is these leaves milling into fine powder [9].

environment. However, this waste is abundant to be used for farm animal food. The need to add value of agricultural waste has been performed by researchers by using them as the reinforcing fibers [7,8] in the composites. For the biodegradable composites, adding high concentration of the oil palm frond could reduce the overall cost for commercial application.

The alkali treatment is usually implemented to improve the compatibility between lignocellulosic fibers and polymeric matrix. According to Wee Lai *et al.* [10], the pretreatment was performed on the lignocellulosic OPF in order to contribute to a significant reduction of lignin and an increase in the cellulose content. The SEM micrographs revealed that the surface of the treated OPF was rough with cavities and disordered internal structures. The rough surface improves the physical interlocking adhesion between treated fibers and polymer matrix. Chen *et al.* [11] reported that the alkali treatment increased the surface roughness of individual bamboo fibers, which the alkali treatment with low NaOH concentration (less than 10%) could enhance the wettability of treated individual bamboo fibers

In this work, OPF waste was milled into fine powder to use as reinforcing agents in poly(lactic acid) (PLA) composites in order to produce biodegradable composites that had good mechanical properties to replace natural wood products. The high content of OPF fibers (30 wt% and 40 wt%) was melt compounded with PLA and fabricated into specimens using a conventional polymer melt processing. The alkali treatment on OPF with various concentrations (1, 3, and 5 wt% of fiber weight) was used to improve the compatibility between polymer and OPF fibers in an inexpensive route. Then, the PLA/OPF composites were studied flexural and tensile properties. Fracture toughness testing was also carried out to compare the improved interfacial adhesion of the alkali-treated OPF fibers. Thermal properties of the PLA/OPF composites were investigated by means of differential scanning calorimetry (DSC) and thermo-gravimetric analysis (TGA). Morphology of the PLA/OPF composites by means of scanning electron microscopy (SEM) was compared with neat PLA in order to analyze the interfacial adhesion of the reinforcing fibers inside the polymer matrix.



Figure 2. Oil palm frond (OPF) fibers obtained by drying oil palm fronds in sunlight (a), grinding leaves into small pieces (b), milling into fine powder (c), and sieving using a sieve shaker (d).

2. Materials and experimental

2.1 Materials

Poly(lactic acid) (PLA) pellets (Ingeo™ Biopolymer 2003D) with MFI of $6 \text{ g} \cdot 10^{-1} \text{ min}$ (210°C, 2.16 kg) was purchased from NatureWork LLC, USA. Oil palm frond (OPF) fibers were kindly supplied by a private company. These OPF fibers were grinded and milled in our laboratory into fine powder.

Then, these fine powder were sieved using a sieve shaker to obtain fiber particles between 140 mesh size (approx. 105 μm) and 200 mesh size (approx. 75 μm). Sodium hydroxide (NaOH, analytical grade) and acetic acid (CH_3COOH , analytical grade) were purchased from Quality Reagent Chemical (QREC), Thailand.

2.2 Alkali treatment of OPF fibers

Sieved OPF fibers were added into the alkali solution having a concentration of 1 wt%, 3 wt%, or 5 wt% of fiber weights. The mixture was mechanical stirred at 175 rpm for 30 min at room temperature. Then, they were washed with distilled water several times and neutralized with acetic acid solution (1M) using a pH meter to monitor the solution's pH until it reached 7. Then, these fibers were filtered and washed again with distilled water several times. Finally, they were thoroughly dried in an air-circulating oven at 80°C for 24 h, and re-grinded using an herb grinder to obtain the alkali-treated OPF fibers.

2.3 Sample compounding and fabrication

Before compounding, PLA pellets and OPF fibers were pre-dried at 60°C for 24 h in an air-circulating oven to remove moisture. Dried PLA pellets and OPF fibers were melt compounded in a co-rotating twin-screw extruder (SHJ-25, Yongteng, China). Table 1 presents sample abbreviations and weight ratios of PLA and OPF used to prepare the composites.

The temperature profile was set as the following: 150°C, 160°C, 170°C, 175°C, 175°C, 180°C, 170°C, and 170°C. The screw speed was set at 48 rpm. The extrudate was water cooled, pelletized, and dried. Dogbone and rectangular specimens were fabricated by an injection moulding machine (Nissei Plastic industrial, Japan) using the temperature profile of 200°C to 230°C from feed zone to nozzle and the mould temperature of 50°C.

Table 1. Compositions of PLA/OPF fibers treated with different concentrations.

Abbreviation	PLA (wt%)	OPF fibers (wt%)	Alkali treatment (wt% of fiber weight)
Neat PLA	100	0	0
PLA70/OPF30_0	70	30	0
PLA70/OPF30_1	70	30	1
PLA70/OPF30_3	70	30	3
PLA70/OPF30_5	70	30	5
PLA60/OPF40_0	60	40	0
PLA60/OPF40_1	60	40	1
PLA60/OPF40_3	60	40	3
PLA60/OPF40_5	60	40	5

Untreated and alkali-treated OPF fibers were characterized by FTIR and TGA. FTIR spectra of OPF fibers were characterized using a FTIR spectrometer (Vertex 70, Bruker, USA). Fibers were mixed with KBr powder and hydraulic pressed into KBr discs. Samples were scanned within the range between 4000 cm^{-1} and 370 cm^{-1} , which the minimum of 32 scans was performed and averaged using a resolution of 4 cm^{-1} . Moreover, thermal property of OPF fibers was characterized using a thermogravimetric analyzer (TGA Perkin Elmer, England) under nitrogen atmosphere. The sample weight used was approximately 5 mg to 10 mg weight. The samples were tested in a heating ramp rate of 10°C·min⁻¹. Temperature scan was performed from 50°C to 800°C. The degradation temperatures and the char residue were recorded and reported.

Flexural testing was performed in accordance to ASTM-D790 using a universal testing machine (Instron model 5969, Instron Engineering Corporation, USA). Rectangular specimens (12.60 cm × 3.00 cm) were tested under the three-point bending mode using a strain rate of 0.01 (crosshead speed of 1.32 mm·min⁻¹). The span length was set at 49.65 mm. The load cell of 5 kN was used. The averages and standard deviations of seven measurements were calculated and reported.

Fracture toughness testing was performed in accordance to ASTM-D5054 using a universal testing machine (Instron, model 5969, Instron Engineering Corporation, USA). Rectangular specimens (12.60 cm × 3.00 cm) were notched and tested under the three-point bending mode in the similar testing condition of the flexural testing. The averages and standard deviations of seven measurements were calculated and reported.

Tensile testing was performed in accordance to ASTM-D638 using a Universal Testing Machine (Instron model 5969, Instron Engineering Corporation, USA). The dogbone (IV-type) specimens were tested using a crosshead speed of 50 mm·min⁻¹. The load cell of 50 kN was used. The averages and standard deviations of eight measurements were calculated and reported.

Thermal properties of neat PLA and PLA/OPF composites were determined using a differential scanning calorimeter (DSC1 Perkin Elmer, England) under nitrogen atmosphere. The sample weight used was approximately 5 mg to 10 mg weight. The samples were tested in a heat-cool-reheat mode, with the heating rate and the cooling rate of 5°C·min. Temperature scan was performed from -40°C to 200°C. The degree of crystallinity (X_c) was calculated as the following equation:

$$\%X_c = \frac{\Delta H_m}{\Delta H_f^0} \times \frac{100}{w} \quad (1)$$

where ΔH_m was melting enthalpy of crystalline ($\text{J}\cdot\text{g}^{-1}$), ΔH_f^0 was melting enthalpy of 100% crystalline of PLA (93.7 $\text{J}\cdot\text{g}^{-1}$) [12], and w was weight fraction of PLA in composites.

Table 2. Compositions of OPF fibers [16] treated with different alkali concentrations.

Possible assignment	Untreated		Alkali treated		
	200 mesh	200+ mesh	1 wt%	3 wt%	5 wt%
-OH stretching vibration	3362	3377	3347	3350	3346
-OH bending vibration	1637	1637	-	-	-
C=O stretching vibration (hemicellulose, lignin)	1736	1736	-	-	-
C=C stretching vibration (aromatic ring in lignin)	1510	1510	1608	1597	1597
C-O stretching vibration (cellulose)	-	-	1057	1058	1059
C-H rocking vibration (cellulose)	898	898	896	896	896

Thermal stability of neat PLA and PLA/OPF composites was also determined using a thermogravimetric analyzer (TGA1 Perkin Elmer, England) under nitrogen atmosphere. The sample weight used was approximately 5 mg to 10 mg weight. The samples were tested in a heating ramp of 10°C·min⁻¹. Temperature scan was performed from 50°C to 800°C. The onset, inflection, and endset temperatures were recorded, and the char residue was also reported.

Morphology of neat PLA and PLA/OPF composites was examined by a Scanning Electron Microscope (SEM) (Tabletop Microscope TM3030, Hitachi, Japan). The moulded specimens were cryo-fractured for observation at the cross-sectional surface. The specimen surface was platinum/gold coated prior to inspection to avoid electrostatic charging.

3. Results and discussion

3.1 Characterization of untreated and alkali-treated OPF fibers

Figure 3 presents the FTIR spectra of untreated and alkali-treated OPF fibers, which Table 2 summarizes the important wavenumbers of these spectra. It is seen that the wavenumber at 1736 cm^{-1} attributed to the C=O stretching (hemicellulose) is absent after the alkali treatment [13]. Also, the wavenumber at 1510 cm^{-1} attributed to the C=C stretching (aromatic ring) is shifted to higher frequency implying the stronger bonding strength. This indicates that the alkali treatment hydrolyzes hemicellulose and lignin leaving cellulose mainly in the OPF fibers. As a result, these alkali-treated OPF fibers are more hydrophilic to be readily compatible with the polyester PLA molecules when melt

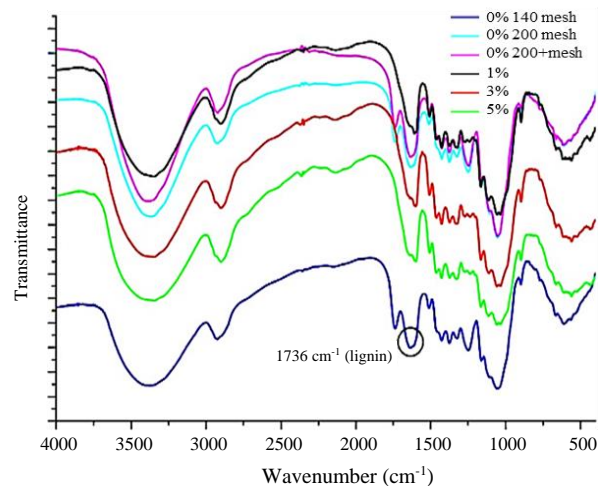
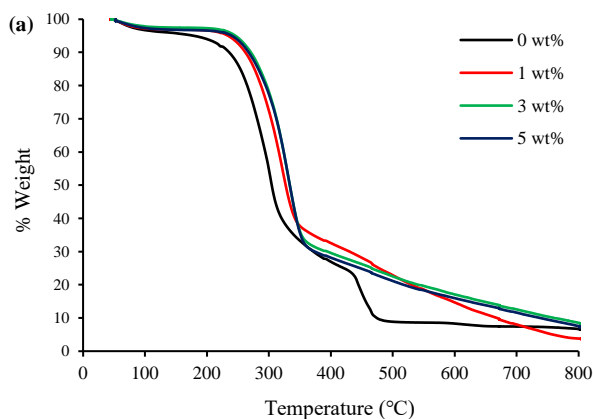


Figure 3. FTIR spectra of untreated and alkali-treated OPF fibers with different alkali concentrations.

compounding. The chemical interaction between the PLA molecules and the lignocellulosic fibers (OPF fibers) is based on the weakly physical interaction between the C=O carbonyl groups in PLA molecules and the -OH groups in celluloses as reported by Qu *et al.* [14]. Mohamad Haafiz *et al.* [15] studied the FTIR spectra of the composites between PLA and the oil palm biomass microcrystalline cellulose (MCC), which they reported that the FTIR spectra of the composites did not reveal any new peak when MCC was added. They suggested that the PLA and MCC only interacted physically rather than chemical interaction.

Figure 4 shows TGA thermogram of untreated and alkali-treated OPF fibers, which the DTG thermogram is also presented for comparison of the degradation temperatures. Untreated OPF fibers had three degradation steps. The first step (264°C to 302°C) was the decomposition of hemicellulose, the second step (302°C to 431°C) was the decomposition of cellulose [16], and the last step (431°C to 442°C) was the decomposition of lignin. Also, the weight loss around 100°C of 4% resulted from the adsorbed moisture in the OPF fibers. After the alkali treatment, the degradation temperature (T_d) was shifted to higher temperature. The first T_d occurred at 279°C, 288°C, and 287°C, and the second T_d occurred at 319°C, 332°C, and 333°C for the alkali treatment of 1 wt%, 3 wt%, and 5 wt%, respectively. This TGA analysis confirmed that lignin was removed as evident by the disappearance of the third T_d , leaving higher concentration of cellulose in the fibers.

Figure 5 shows physical appearance of neat PLA and PLA/OPF composites reinforced with untreated or alkali-treated OPF fibers.



Under natural light, the PLA specimen is seen as glossy-translucent while the PLA/OPF composite specimens are dull dark-brownish with rough surface. The alkali concentration did not have influence on the color significantly when adding such high content of OPF fibers (30 wt% or 40 wt%).

It was reported that alkali treatment of Ironwood fibers produced PLA-based composites with hardwood-like (texture /sense), which the alkali-treated Ironwood fibers was dark reddish-brown and the color of the composites became darker brown after melt compounding [17]. The surface of the composites was rougher with the higher fiber concentration. With the OPF fiber of 40 wt%, the dimension of the injection molded specimens was slightly smaller than the neat PLA due to higher melt viscosity [18] that required the higher holding pressure or holding time to complete the shrinkage of the molded parts.

3.2 Flexural properties of untreated and alkali-treated PLA/OPF composites compared with neat PLA

Figure 6 presents flexural modulus, flexural strength, and flexural strain at break of neat PLA and PLA/OPF composites. Table 3 summarizes flexural properties of neat PLA and PLA/OPF composites which the increase of modulus in percentage is calculated to compare with neat PLA's modulus. The neat PLA had flexural modulus of about 3863 MPa, which the flexural strength was 91 MPa and the strain at break was 6.46 mm·mm⁻¹.

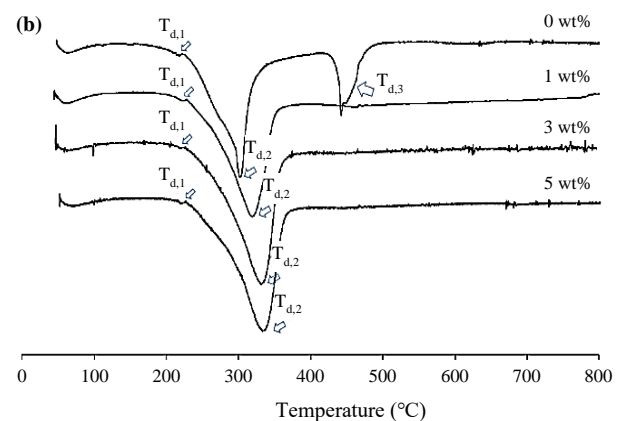


Figure 4. TGA (a) and DTG (b) thermograms of untreated and alkali-treated OPF fibers with different alkali concentrations.

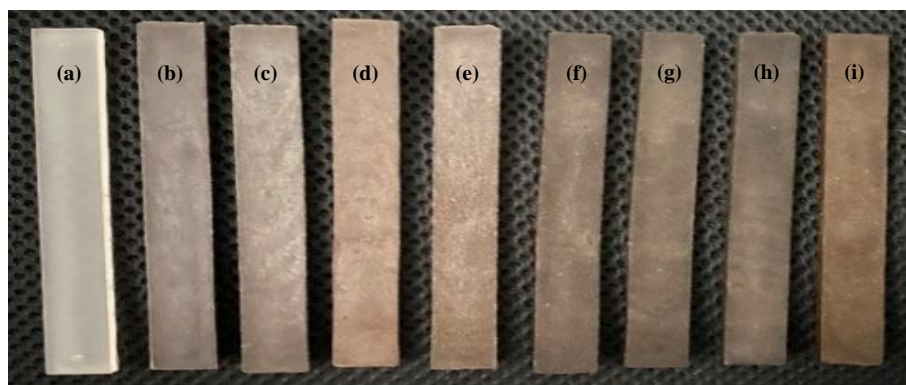


Figure 5. Physical appearance of neat PLA (a) and PLA-based composites adding untreated and alkali-treated OPF fibers of 30 wt% (b-e), and 40 wt% (f-i).

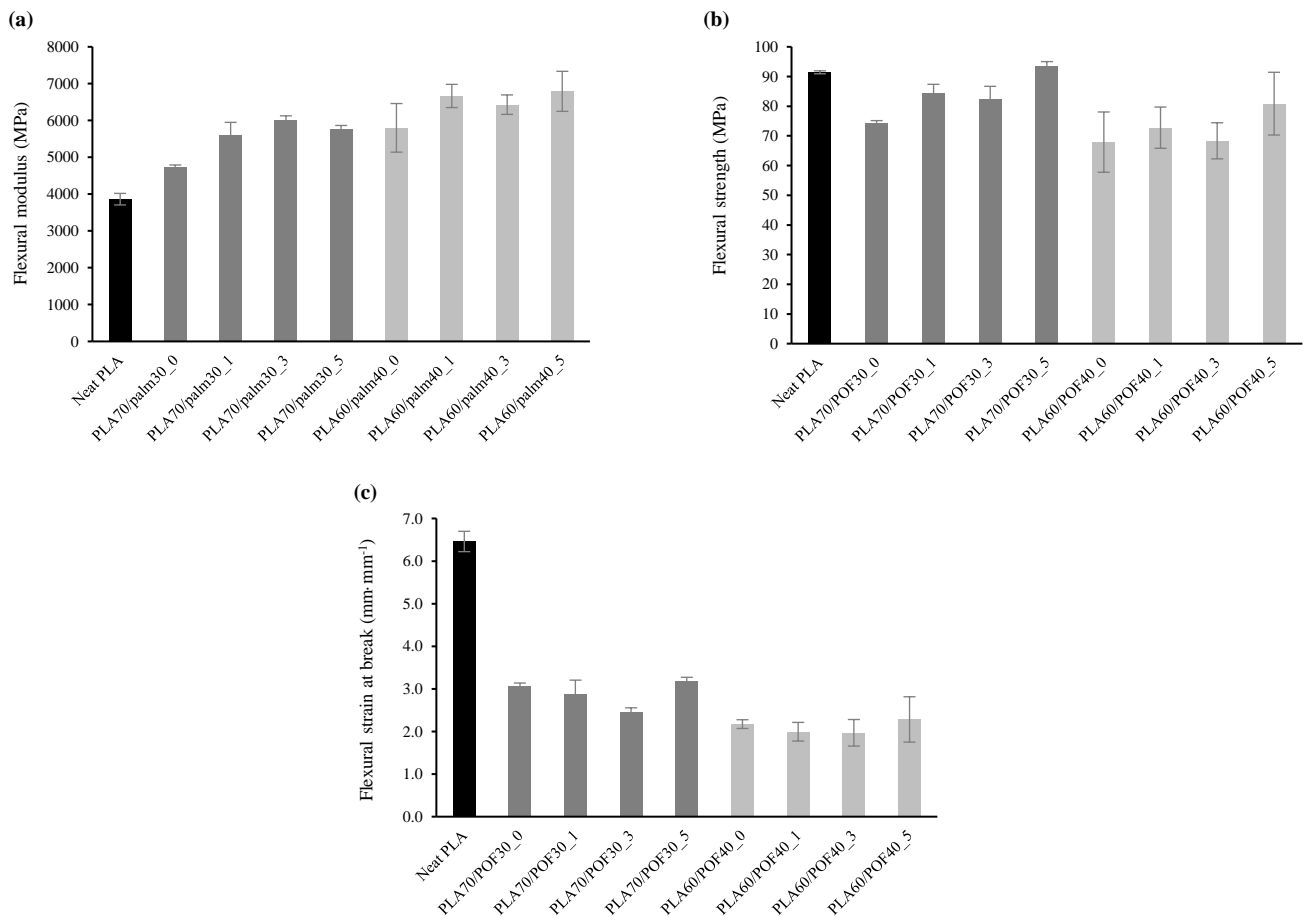


Figure 6. Flexural modulus (a), flexural strength (b), and flexural strain at break (c) of neat PLA and PLA/OPF composites adding untreated and alkali-treated OPF fibers of 30 wt% and 40 wt%.

Table 3. Flexural properties of neat PLA and PLA/OPF composites adding untreated and alkali-treated OPF fibers of 30 wt% and 40 wt%.

Sample	Flexural modulus (MPa)	Increase of modulus compared with neat PLA (%)	Flexural strength (MPa)	Flexural strain at break ($\text{mm}\cdot\text{mm}^{-1}$)
Neat PLA	$3,862.84 \pm 156.76$	0.00	91.42 ± 0.50	6.46 ± 0.24
PLA70/OPF30_0	$4,742.11 \pm 49.16$	22.7	74.29 ± 0.85	3.06 ± 0.08
PLA70/OPF30_1	$5,612.78 \pm 335.38$	45.3	84.35 ± 3.02	2.87 ± 0.34
PLA70/OPF30_3	$6,013.57 \pm 112.55$	55.7	82.50 ± 4.19	2.45 ± 0.11
PLA70/OPF30_5	$5,761.28 \pm 102.85$	49.2	93.65 ± 1.37	3.19 ± 0.08
PLA60/OPF40_0	$5,799.95 \pm 659.96$	50.2	67.90 ± 10.16	2.17 ± 0.10
PLA60/OPF40_1	$6,665.47 \pm 315.32$	72.6	72.76 ± 6.95	1.99 ± 0.22

Compounding PLA with untreated OPF fibers increased flexural modulus of the composites significantly. Depending on alkali concentration, compounding alkali-treated OPF fibers from oil palm frond waste of 30 wt% and 40 wt% could increase flexural modulus to be 55% and 75% higher compared to that of neat PLA, respectively. The stiffness enhancement was similar to the date palm fiber reinforced polyester composite prepared by the work of Al-Kaabi *et al.* [19] Comparison among them, flexural modulus and flexural strength of the PLA/OPF30wt% composites were increased with alkali concentration for the fiber surface treatment. This correlated to the increase of total breaking energy by the fracture toughness testing attributed to the interfacial adhesion between phases. Meanwhile, flexural modulus of the PLA/OPF40wt% composites was almost

independent of alkali concentration but was higher than those adding untreated fibers.

3.3 Fracture toughness properties of untreated and alkali-treated PLA/OPF composites compared with neat PLA

The interfacial adhesion between polymer matrix and reinforcing fibers is one of the crucial factors to obtain the optimum mechanical properties. In order to analyze the bonding strength, the fracture toughness testing was carried out onto flexural specimens having notch under a constant crosshead speed. The maximum flexure strength and total breaking energy of neat PLA and alkali-treated PLA/OPF composites adding OPF fibers of 30 wt% and 40 wt%

are presented in Figure 7, which Table 4 summarizes the average fracture toughness properties and their standard deviations.

It was found that neat PLA had the highest maximum flexure strength and total breaking energy, which the specimens were broken in hinge mode due to ductile behaviour under low strain rate. The PLA/OPF composites were broken in either hinge or complete break mode as shown in Figure 7(c).

For those broken in hinge mode, this implied that there was plenty of PLA matrix at the specimen skin to inhibit the crack propagation. For complete break mode, this indicated the fibers acting as the stress concentrators to initiate crack at the interphases. Since these specimens of the PLA/OPF composites were all fractured during

the fracture toughness testing, the trend of the maximum flexure strength and total breaking energy was similar to those obtained from the flexural testing. When the alkali concentration increased, the increase of maximum flexure strength confirmed the improved interfacial adhesion between PLA matrix and treated fibers.

The total breaking energy of the notched specimens increased with respect to the alkali concentration due to the better adhesion between polymer matrix and the fibers. However, the total breaking energy of the PLA/OPF composites reduced when increasing the fiber content. This emphasized the notch sensitivity of the PLA/OPF composites compared to the neat PLA.

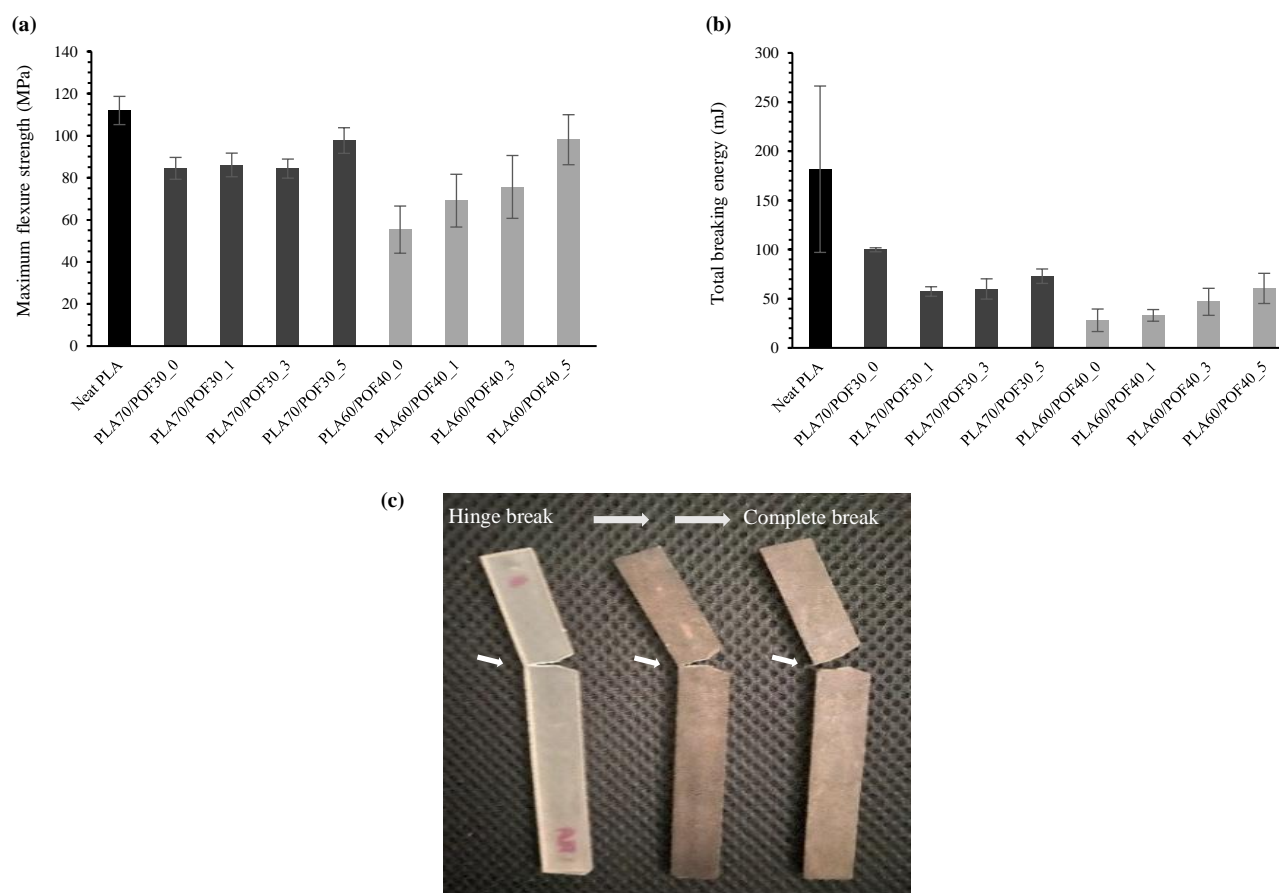


Figure 7. Maximum flexure strength (a), total breaking energy (b), and breakage mode (c) of neat PLA and PLA/OPF composites adding untreated and alkali-treated OPF fibers of 30 wt% and 40 wt%.

Table 4. Fracture toughness properties of neat PLA and PLA/OPF composites adding untreated and alkali-treated OPF fibers of 30 wt% and 40 wt%.

Sample	Maximum flexure strength (MPa)	Flexure strain ($\text{mm}\cdot\text{mm}^{-1}$)	Total breaking energy (mJ)
Neat PLA	111.97 \pm 6.71	1.07 \pm 0.22	181.72 \pm 84.6
PLA70/OPF30_0	84.47 \pm 5.19	0.72 \pm 0.05	99.80 \pm 2.04
PLA70/OPF30_1	86.09 \pm 5.62	0.56 \pm 0.07	57.37 \pm 4.83
PLA70/OPF30_3	84.35 \pm 4.54	0.52 \pm 0.10	59.93 \pm 10.31
PLA70/OPF30_5	97.70 \pm 6.09	0.69 \pm 0.09	72.92 \pm 7.33
PLA60/OPF40_0	55.34 \pm 11.21	0.39 \pm 0.22	28.08 \pm 11.45
PLA60/OPF40_1	69.11 \pm 12.54	0.52 \pm 0.14	33.07 \pm 5.92
PLA60/OPF40_3	75.64 \pm 14.94	0.54 \pm 0.16	46.85 \pm 13.75
PLA60/OPF40_5	98.08 \pm 11.89	0.55 \pm 0.18	60.49 \pm 15.34

3.4 Tensile properties of untreated and alkali-treated PLA/OPF composites compared with neat PLA

Figure 8 presents tensile properties of neat PLA and PLA/OPF composites. Similarly, Young's modulus of PLA/OPF composites increased with respect to OPF fibers, which the composites adding alkali-treated OPF fibers had higher modulus than those adding untreated fibers. Tensile strength at break of the PLA/OPF composites was lower than neat PLA implying the insufficient interfacial adhesion between PLA and OPF fibers. However, tensile strength at break of the alkali-treated PLA/OPF30wt% composites showed the influence of alkali concentration to improve the interfacial adhesion between phases, which the composites adding the OPF fibers treated with the alkali concentration of 5 wt% showed the highest tensile strength at break that was higher than that of neat PLA. In contrast, the tensile strength at break of the PLA/OPF40wt% composite was reduced significantly indicating that the failure occurred at the interphase due to the stress concentration effect.

3.5 Thermal characterization of PLA/OPF composites adding untreated and alkali-treated OPF fibers compared with neat PLA

Figure 9 shows the glass transition temperatures (T_g) and enthalpy of fusion under the melting peaks at 146°C to 147°C and 153°C to

154°C of neat PLA and PLA/OPF composites adding untreated and alkali-treated OPF fibers of 30 wt% and 40 wt%, which Table 6 summarizes the data obtained from the DSC analysis from the 2nd heating scan.

It was found that PLA showed the T_g at 58.80°C, which the T_g was reduced significantly in the PLA/OPF composites as shown in the trend line in the figure. Since the reduction of T_g could be used to indicate the lower molecular weight of polymer, this implies that the chain scission of PLA molecules occurred significantly when compounding with OPF fibers. It was possibly that the adsorbed moisture in the OPF fibers (as evident in TGA results) would generate hydrolysis of the polyester with the alkali trace acted as the catalyst. However, the T_g increased with the concentration of alkali treatment implying the improvement of interfacial adhesion between the polymer matrix and OPF fibers that restricted the mobility of the PLA molecules in the amorphous region.

From the DSC analysis, it was found that there were two melting peaks showing at the temperature at 146°C to 147°C and at 153°C to 154°C. These melting peaks indicated the different crystal forms and perfection. Zhang *et al.* [20] studied melt crystallization behavior of PLA/PCL blends compatibilized by Lactide-Caprolactone copolymer. They reported that the addition of PCL increased the nuclei density, which the spherulite size became smaller than that of the neat PLA, and the blends under the isothermal crystallization at various temperature showed the imperfection of crystals causing change of melting enthalpy

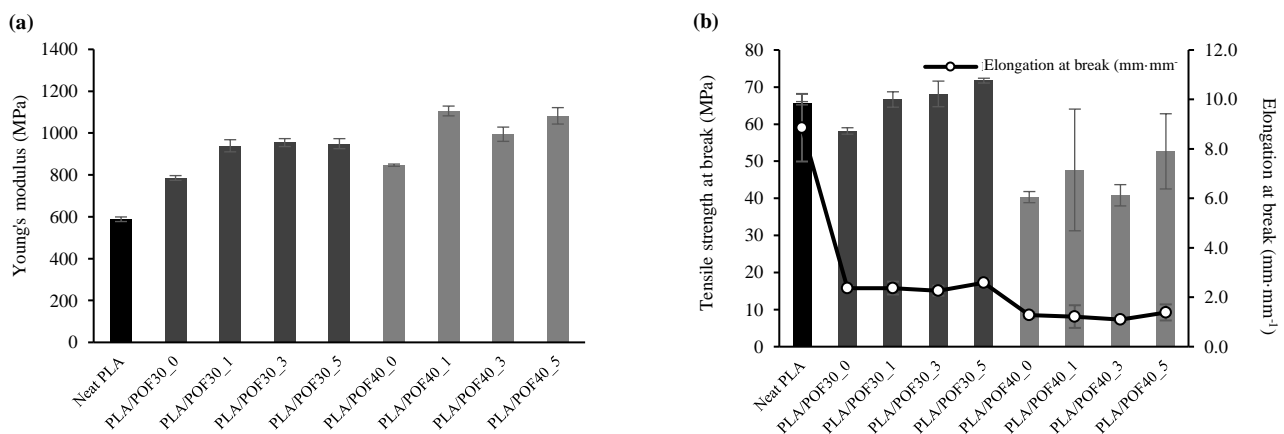


Figure 8. Tensile modulus (a), tensile strength at break and elongation at break (b) of neat PLA and PLA/OPF composites adding untreated and alkali-treated OPF fibers of 30 wt% and 40 wt%.

Table 5. Tensile properties of neat PLA and PLA/OPF composites adding untreated and alkali-treated OPF fibers of 30 wt% and 40 wt%.

Sample	Tensile modulus (MPa)	Tensile strength at break (MPa)	Elongation at break (mm·mm ⁻¹)
Neat PLA	588.32 ± 11.00	65.65 ± 0.44	8.86 ± 1.37
PLA70/OPF30_0	785.48 ± 11.41	58.17 ± 0.87	2.37 ± 0.07
PLA70/OPF30_1	939.28 ± 28.94	66.65 ± 2.07	2.37 ± 0.26
PLA70/OPF30_3	954.53 ± 18.97	68.16 ± 3.45	2.27 ± 0.20
PLA70/OPF30_5	949.51 ± 23.90	71.74 ± 0.65	2.59 ± 0.13
PLA60/OPF40_0	846.61 ± 5.23	40.33 ± 1.50	1.28 ± 0.11
PLA60/OPF40_1	1105.62 ± 23.42	47.66 ± 16.41	1.22 ± 0.46
PLA60/OPF40_3	994.46 ± 34.05	40.82 ± 2.87	1.10 ± 0.08
PLA60/OPF40_5	1082.36 ± 39.27	52.67 ± 10.14	1.39 ± 0.32

Table 6. Data from the 2nd heating scan of DSC showing glass transition temperatures (T_g), cold crystallization temperatures (T_{cc}), crystal melting temperatures (T_m), enthalpy of fusion (ΔH_m), and the degree of crystallinity (X_c) of neat PLA and PLA/OPF composites adding untreated and alkali-treated OPF fibers of 30 wt% and 40 wt%.

Sample	T_g (°C)	T_{cc} (°C)	ΔH_{cc} (J·g ⁻¹)	$T_{m,1}$ (°C)	$T_{m,2}$ (°C)	$\Delta H_{m,1}$ (J·g ⁻¹)	$\Delta H_{m,2}$ (J·g ⁻¹)	X_c (%)
Neat PLA	58.80	109.84	-20.412	147.34	153.03	8.386	1.549	15.15
PLA70/OPF30_0	57.36	111.93	-20.487	146.94	153.20	9.640	4.710	21.88
PLA70/OPF30_1	57.54	107.75	-18.575	146.35	153.45	8.202	6.919	23.05
PLA70/OPF30_3	57.69	107.77	-17.648	146.78	154.03	7.606	7.721	23.37
PLA70/OPF30_5	58.03	107.84	-17.303	146.76	153.62	7.489	6.335	21.08
PLA60/OPF40_0	56.01	103.58	-17.291	144.93	152.70	5.860	9.093	22.80
PLA60/OPF40_1	56.51	104.59	-15.486	145.27	153.20	5.931	9.388	23.36
PLA60/OPF40_3	57.20	106.68	-17.310	146.27	153.70	6.391	8.859	23.25
PLA60/OPF40_5	57.44	108.76	-16.497	146.85	154.11	7.004	7.225	21.69

and the degree of crystallinity. As seen in Table 6, the incorporation of OPF fibers also influenced the cold crystallization (T_{cc}) of the PLA matrix, which the T_{cc} of the PLA/OPF composites occurred at the significant lower temperature. From the cooling scan, the crystallization temperature was not clearly observed due to the slow crystallinity of the PLA molecules. Then, the PLA molecules initiated the T_{cc} at 109.8°C during the 2nd heating scan, and the alkali treated OPF fibers became the nucleating sites for the PLA crystals to continue their crystal growth.

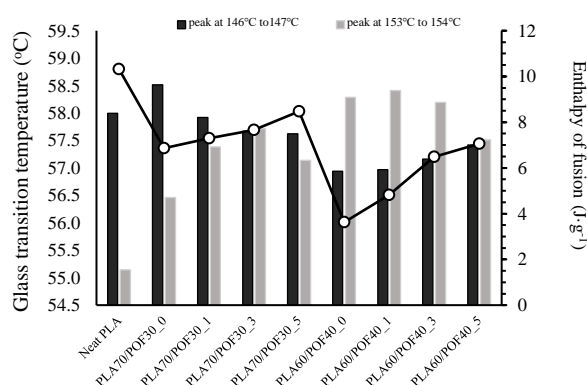


Figure 9. Glass transition temperatures and enthalpy of fusion under the melting peaks at 146°C to 147°C and 153°C to 154°C of neat PLA and PLA/OPF composites adding untreated and alkali-treated OPF fibers of 30 wt% and 40 wt%.

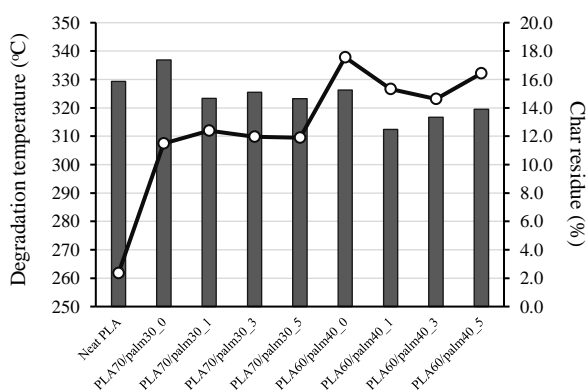


Figure 10. Degradation temperatures (inflection point) and char residue of neat PLA and PLA/OPF composites adding untreated and alkali-treated OPF fibers of 30 wt% and 40 wt%.

In this research, the trend of the area under peaks are presented in Figure 9. The degree of crystallinity increased in the PLA/OPF composites, but did not show the correlation with the fiber content. However, the second peak increased with respect to the alkali concentration for the PLA/OPF 30wt% composites, while it was almost constant for the PLA/OPF 40wt% composites. This could be attributed to the shorter molecular chains of PLA (resulted from chain scission) promoted the nucleation but the OPF inhibited the crystal growth. The improvement of interfacial adhesion between PLA matrix and OPF fibers improved the perfection of the PLA crystals.

3.6 Thermal stability of PLA/OPF composites adding untreated and alkali-treated OPF fibers compared with neat PLA

Figure 10 presents thermal stability of PLA/OPF composites adding untreated and alkali-treated OPF fibers compared with neat PLA. Basically, adding OPF fibers reduced the degradation temperatures (T_d) of the composites due to the induction of the thermal decomposition of OPF fibers at about 280°C (onset degradation temperature). The free radical products of the fiber degradation could initiate the chain scission of the PLA molecules to occur at lower temperature.

The PLA/OPF composites adding 40 wt% OPF fibers had lower T_d than those adding 30 wt%. The char residue of neat PLA was about 2.35 wt% due to aliphatic structure of PLA. Unsurprisingly, the char residue of the PLA/OPF composites was higher when adding OPF fibers, which the final weight (about 10-15 wt%) would correlate to the lignin content.

3.7 Morphology of PLA/OPF composites adding untreated and alkali-treated OPF fibers compared with neat PLA

Figure 11 presents SEM micrographs of cryofracture surface of neat PLA and PLA/OPF composites adding untreated and alkali-treated OPF fibers. Under 500x magnification, the fracture surface of neat PLA showed localized yielding and cracking that propagated parallel resemble the brittle failure. For the untreated PLA/OPF composites, voids were observed at the interface between PLA matrix and fibers indicating the limited wetting due to the difference of chemical affinity. The wettability of the PLA matrix onto the alkali-treated OPF fibers was improved attributed to the increase of hydrophilicity. The composite fracture surface was rougher indicating the crack propagation pathway

was various due to these reinforced fibers became the stress concentrators. There were some traces in the PLA matrix indicating that fibers were peeled-out from the PLA matrix. This implied that the alkali-treated OPF fibers attached well with the PLA matrix until the stress was

high enough to pull them out. From these observations, the alkali-treated OPF could reinforce the PLA matrix to enhance flexural and tensile modulus of the composites.

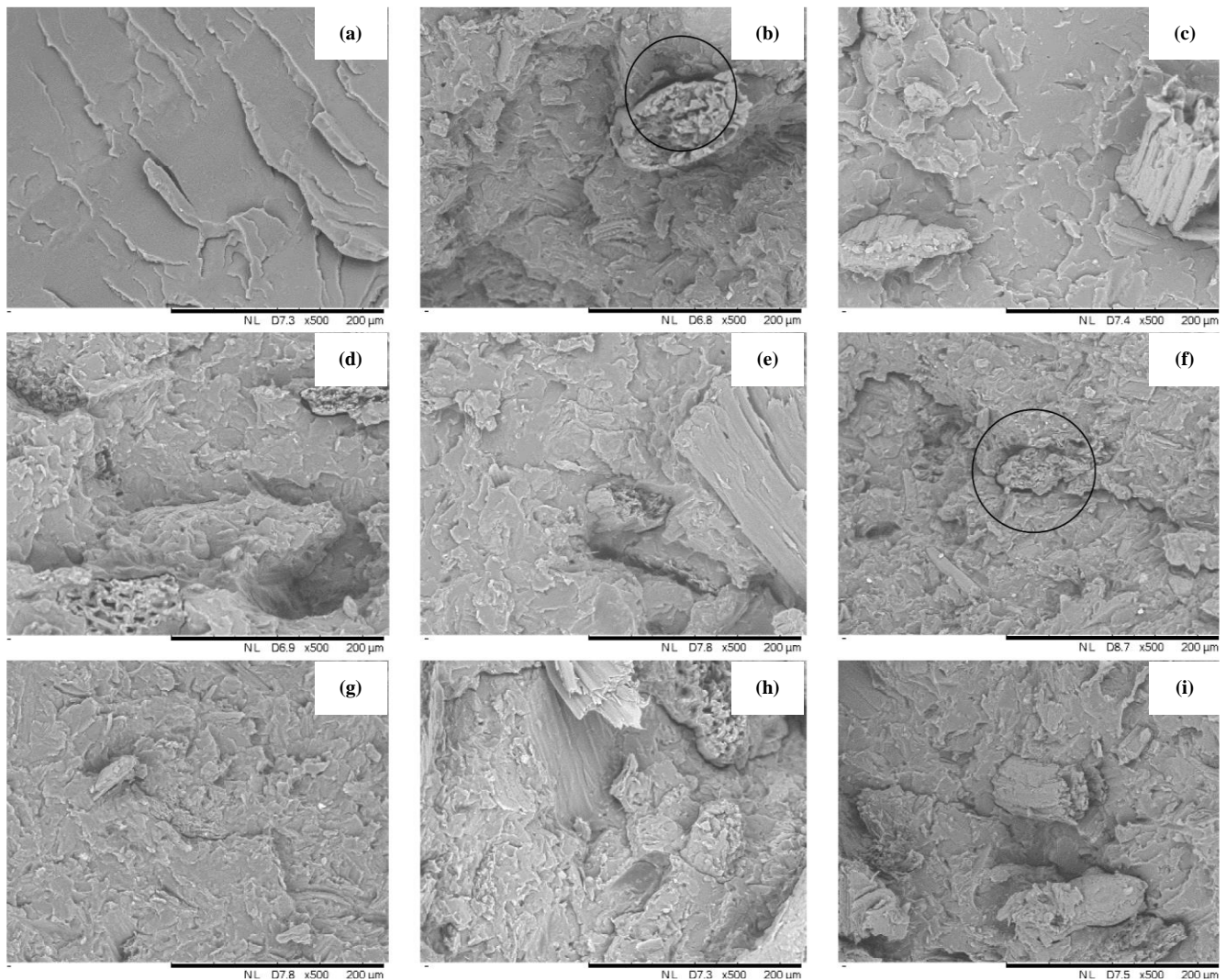


Figure 11. SEM micrographs (magnification 500x) of cryofracture surface of neat PLA (a), PLA70/OPF30_0 (b), PLA70/OPF30_1 (c), PLA70/OPF30_3 (d), PLA70/OPF30_5 (e), PLA60/OPF40_0 (f), PLA60/OPF40_1 (g), PLA60/OPF40_3 (h), and PLA60/OPF40_5 (i).

4. Conclusions

Green composites for sustainable application were successfully prepared and investigated the properties. The alkali treated OPF fibers of 30 wt% or 40 wt% were compounded with PLA in a twin-screw extruder and injection moulded into testing specimens. The alkali concentrations for fiber surface treatment were 0 wt%, 1 wt%, 3 wt%, and 5 wt%. It was found that the alkali treated OPF fiber PLA adding 30 wt% and 40 wt% composites had the flexural modulus to be about 55% and 75% higher than those without the treatment, respectively. This was due to the better compatibility between phases indicated by the better wettability and lesser voids as shown in SEM micrographs. The glass transition temperature (T_g) of PLA matrix in the composites was shifted to lower temperature attributed to the thermal degradation of PLA during the melt compounding which

confirmed by the lower degradation temperature. Increasing the alkali concentration caused the T_g to be higher implying the improvement of interfacial adhesion. Nevertheless, the higher rigidity PLA/OPF composites became more brittle as evident by the fracture toughness testing, which the increase of breaking energy confirmed the better interfacial adhesion between phases.

Acknowledgement

The authors would like to thank the Department of Materials Science and Engineering, Faculty of Engineering and Industrial Technology, Silpakorn University for fully funding this research. The authors also thank Ms. Phattaramon Sriphattarapan and Mr. Kiattisak Sophon for performing the TGA and the DSC testing, respectively.

References

- [1] I. Vroman, and L. Tighzert, "Biodegradable polymers," *Materials*, vol. 2, pp. 307-344, 2009.
- [2] A. Arbelaiz, U. Txueka, I. Mezo, and A. Orue, "Biocomposites based on poly(lactic acid) matrix and reinforced with lignocellulosic fibers: the effect of fiber type and matrix modification," *Journal of Natural Fibers*, 2020.
- [3] C. G. Silva, P. A. L. Campini, D. B. Rochaa, and D. S. Rosa, "The influence of treated eucalyptus microfibrils on the properties of PLA biocomposites," *Composites Science and Technology*, vol. 179, pp. 54-62, 2019.
- [4] H. Peltola, K. Immonen, L. S. Johansson, J. Virkajärvi, and D. Sandquist, "Influence of pulp bleaching and compatibilizer selection on performance of pulp fiber reinforced PLA biocomposites," *Journal of applied polymer science*, vol. 136, no. 37, pp. 47955, 2019.
- [5] S. D. S. Kopparchy, and A. N. Netravali, "Review: Green composites for structural applications," *Composites Part C*, vol. 6, pp. 100169, 2021.
- [6] N. Laemsak, and M. Okuma, "Development of boards made from oil palm frond II: properties of binderless boards from steam-exploded fibers of oil palm frond," *Journal of wood science*, vol. 46, no. 4, pp. 322-326, 2012.
- [7] A. E. Eladawi, and A. H. Rajpar, "Investigation of mechanical properties for reinforced polyester composites with palm fronds," *Journal of Materials Science and Chemical Engineering*, vol. 8, pp. 74-84, 2020.
- [8] M. Russita, and Bahruddin, "Production of palm frond based wood plastic composite by using twin screw extruder," *IOP Conference Series: Materials Science and Engineering*, vol. 345, pp. 012039, 2018.
- [9] D. Maheshwari, *Composting for Sustainable Agriculture (Sustainable Development and Biodiversity)*. 2014.
- [10] W. Long, L. W. Lai, N. M. Rahim, E. F. Hashim, Z. Ya'cob, A. Idris, and J. Akhtar, "Study on composition, structural and property changes of oil palm frond biomass under different pretreatments," *Cellulose Chemistry and Technology*, vol. 50, pp. 951-959, 2016.
- [11] H. Chen, W. Zhang, X. Wang, H. Wang, Y. Wu, T. Zhong, and B. Fei, "Effect of alkali treatment on wettability and thermal stability of individual bamboo fibers," *Journal of Wood Science*, vol. 64, pp. 398-405, 2018.
- [12] E. Quero, A. J. Müller, F. Signori, M. B. Coltelli, and S. Bronco, "Isothermal cold-crystallization of PLA/PBAT blends with and without the addition of Acetyl Tributyl Citrate," *Macromolecular Journal*, vol. 213, pp. 36-48, 2012.
- [13] S.-N. Sun, X.-F. Cao, H.-Y. Li, F. Xu, and R.-C. Sun, "Structural characterization of residual hemicelluloses from hydrothermal pretreated Eucalyptus fiber," *International Journal of Biological Macromolecules*, vol. 69, pp. 158-164, 2014.
- [14] P. Qu, Y. Goa, G. F. Wu, and L. P. Zhang, "Nanocomposite of poly(lactic acid) reinforced with cellulose nanofibrils," *BioResources*, vol. 5, no. 3, pp. 1811-1823, 2010.
- [15] M. K. Mohamad Haafiz, Azman Hassan, Zainoha Zakaria, I. M. Inuwa, M. S. Islam, and M. Jawaid, "Properties of polylactic acid composites reinforced with oil palm biomass microcrystalline cellulose," *Carbohydrate Polymers*, vol. 98, no. 1, pp. 139-145, 2013.
- [16] N. A. Nordin, O. Sulaiman, R. Hashim, and M. H. M. Kassim, "Oil palm frond waste for the production of cellulose nanocrystals," *Journal of Physical Science*, vol. 28, no. 2, pp. 115-126, 2017.
- [17] N. Hongsriphan, "Influence of chemical treatment and fiber content on color and properties of renewable wood composite using Ironwood saw dust," in *The 2016 Pure and Applied Chemistry International Conference (PACCON 2016)*, BITEC, Bangkok, T. Vilaivan, Ed., 9-11 February 2016: The Chemical Society of Thailand under the Patronage of Professor Dr. HRH Princess Chulabhorn, pp. 1217-1222.
- [18] A. Leao, R. M. F. Teixeira, and P. Ferrão, "Production of reinforced composites with natural fibers for industrial applications – extrusion and injection WPC," *Molecular Crystals and Liquid Crystals*, vol. 484, no. 1, pp. 157-166, 2008.
- [19] K. Al-Kaabi, A. Al-Khanbashi, and A. Hammami, "Natural fiber reinforced composites from Date palm fibers " in *11th European Conference on Composite Materials : from Nano-scale Interactions to Engineering Structures*, Rhodes, Greece, C. Galiotis, Ed., May 31 - June 3, 2004.
- [20] C. Zhang, Q. Lan, T. Zhai, S. Nie, J. Luo, and W. Yan, "Melt crystallization behavior and crystalline morphology of polylactide/poly(ϵ -caprolactone) blends compatibilized by Lactide-Caprolactone copolymer," *Polymers*, vol. 10, pp. 1181, 2018.